Differences in Enantioselective Hydroxylation of 2,2′,3,6-Tetrachlorobiphenyl (CB45) and 2,2′,3,4′,6-Pentachlorobiphenyl (CB91) by Human and Rat CYP2B Subfamilies

Inui, Hideyuki ; Ito, Terushi ; Miwa, Chiharu ; Haga, Yuki ; Kubo, Makoto ; Itoh, Toshimasa ; Yamamoto, Keiko ; Miyaoka, Masayuki ; Mori,…

(Citation)
Environmental Science & Technology,56(14):10204-10215

(Issue Date)
2022-07-19

(Resource Type)
journal article

(Version)
Accepted Manuscript

Differences in enantioselective hydroxylation of 2,2′,3,6-tetrachlorobiphenyl (CB45) and 2,2′,3,4′,6-pentachlorobiphenyl (CB91) by human and rat CYP2B subfamilies

Hideyuki Inui[1,2,*], *Terushi Ito*[2], *Chiharu Miwa*[3], *Yuki Haga*[4], *Makoto Kubo*[5], *Toshimasa Itoh*[5], *Keiko Yamamoto*[5], *Masayuki Miyaoka*[6], *Tadashi Mori*[6], *Harunobu Tsuzuki*[2], *Shintaro Mise*[2], *Erika Goto*[2], *Chisato Matsumura*[4], *Takeshi Nakano*[7]

[1]Biosignal Research Center, Kobe University, 1-1 Rokkodaicho, Nada-ku, Kobe, Hyogo 657-8501, Japan

[2]Graduate School of Agricultural Science, Kobe University, 1-1 Rokkodaicho, Nada-ku, Kobe, Hyogo 657-8501, Japan

[3]Faculty of Agriculture, Kobe University, 1-1 Rokkodaicho, Nada-ku, Kobe, Hyogo 657-8501, Japan

[4]Hyogo Prefectural Institute of Environmental Sciences, 3-1-18 Yukihiracho, Suma-ku, Kobe, Hyogo 654-0037, Japan

[5]Laboratory of Drug Design and Medicinal Chemistry, Showa Pharmaceutical University, 3-3165 Higashi-Tamagawagakuen, Machida, Tokyo 194-8543, Japan

[6]Graduate School of Engineering, Osaka University, 2-1 Yamadaoka, Suita, Osaka 565-0871, Japan

[7]Research Center for Environmental Preservation, Osaka University, 2-4 Yamadaoka, Suita, Osaka 565-0871, Japan

*Corresponding Author

Hideyuki Inui, Biosignal Research Center, Kobe University, 1-1 Rokkodaicho, Nada-ku, Kobe, Hyogo, 657-8501, Japan

E-mail: hinui@kobe-u.ac.jp, Telephone number: +81-78-803-5863

KEYWORDS: Atropisomer, chiral polychlorinated biphenyl, cytochrome P450 monooxygenase, docking model, enantioselectivity, hydroxylation, 2,2′,3,4′,6-pentachlorobiphenyl, 2,2′,3,6-tetrachlorobiphenyl

SYNOPSIS

Each atropisomer of CB45 and CB91 was enantioselectively metabolized by human CYP2B6 and rat CYP2B1. These metabolites were predicted by designing docking models.

ABSTRACT

Although polychlorinated biphenyls (PCBs) were commercially banned half a century ago, contamination of the environment and organisms by PCBs is still observed. PCBs show high persistency and bioaccumulation, resulting in toxicity. Among PCBs, chiral PCBs with more than three chlorine atoms at the *ortho*-position exhibit developmental and neurodevelopmental toxicity. Because toxicity is dependent on the atropisomer, atropisomer-specific metabolism is vital in determining toxicity. However, structural information on enantioselective metabolism remains elusive. Cytochrome P450 (CYP, P450) monooxygenases, particularly human CYP2B6 and rat CYP2B1, metabolize separated atropisomers of 2,2′,3,6-tetrachlorobiphenyl (CB45) and 2,2′,3,4′,6-pentachlorobiphenyl (CB91) to dechlorinated and hydroxylated metabolites. Docking studies using human CYP2B6 predict 4′-hydroxy (OH)-CB45 from (a*R*)-CB45 as a major metabolite of CB45. Di-OH- and dechlorinated OH-metabolites from human CYP2B6 and rat CYP2B1 are also detected. Several hydroxylated metabolites are derived from CB91 by both P450s; 5-OH-CB91 is predicted as a major metabolite. CB91 dechlorination is also detected by identifying 3-OH-CB51. Stable conformation of PCBs in the substrate-binding cavity and close distance to P450 heme are responsible for high metabolizing activities. As hydroxylation and dechlorination change PCB toxicity, this approach helps understand the possible toxicity of chiral PCBs in mammals.

1. INTRODUCTION

Cytochrome P450 (CYP, P450) monooxygenases are primarily involved in the metabolism of xenobiotic compounds in organisms. These reactions, such as hydroxylation, dealkylation, and dehalogenation of the compounds, influence their fate. For example, toxic foreign compounds are easily excreted from the body after reactions with P450s, resulting in decreased toxicity.[1] CYP-mediated transformation products allow for conjugation with hydrophilic moieties in further excretion mechanisms, such as Phase II reactions. Polychlorinated biphenyls (PCBs) are ubiquitously detected in the environment and organisms because they show remarkable persistency and bioaccumulation owing to their high hydrophobicity. Hereby, it is known that PCBs are one of the most serious anthropogenic pollutants and are registered as persistent organic pollutants.[2] PCB toxicity is often expressed as dioxin-like toxicity, which includes carcinogenicity, teratogenicity, and immunotoxicity, mediated by an aryl hydrocarbon receptor.[3] Although this type of toxicity is particularly caused by dioxin-like PCBs with one or no chlorine atoms at the *ortho*-position of PCBs, neurodevelopmental toxicity in particular is induced by chiral PCBs.[4] The atropisomerism in PCBs occurs in cases where at least one *ortho*-position of each ring bears a chlorine atom. Chiral PCBs are composed of two atropisomers that are non-superimposable mirror images. These have the same physical and chemical properties and exist at a 1:1 ratio in a commercial chiral PCB. However, biased ratios are often observed in the environment[5] and organisms, such as earthworms,[6] zebrafish,[7] and whales,[8] as well as in humans.[9] This ratio change is caused by metabolism, and it unleashes the atropisomer-specific toxicity of chiral PCBs. Atropisomer-specific stress responses are often observed. The contents of amino acids and lipids decrease in earthworms treated with (+)-2,2′,3,4′,6-pentachlorobiphenyl (CB91) but not after treatment with (–)-CB91,[6] and some antioxidant enzyme genes are suppressed in zebrafish brains treated with (–)-CB91.[7] Furthermore, atropisomer-specific toxicity has been reported to result in

78 higher mortality in adult zebrafish treated with (–)-CB91 than those treated with (+)-CB91,[10]
79 and the exposure of rats with (–)-2,2′,3,3′,6,6′-hexachlorobiphenyl (CB136) leads to adverse
80 neurodevelopmental outcomes due to binding to a ryanodine receptor (RyR).[11] Although it is
81 known that decrease in one atropisomer due to enantioselective metabolism by P450s becomes a
82 critical point to express toxicity, the underlying mechanisms remain unclear. 2,2′,4,6′-
83 Tetrachlorobiphenyl (CB51) has been enantioselectively metabolized to 3′-hydroxy (OH)-CB51
84 with approximately 0.2 of the enantiomeric fraction (EF) and 3′,4′-diOH-CB51 by microsomes
85 from rats treated with the CYP2B subfamily inducer phenobarbital.[12] Chiral pentachlorobiphenyls,
86 such as CB91 and 2,2′,3,5′,6-pentachlorobiphenyl (CB95), have also been hydroxylated in liver
87 tissue slices prepared from mice treated with phenobarbital.[13] Human CYP2B6 produced 5-OH-
88 CB91 than 4-OH-CB91 and 3-OH-2,2′,4,4′,6-pentachlorobiphenyl (3-OH-CB100).[14] These results
89 strongly suggest that the CYP2B subfamily, particularly human CYP2B6 and rat CYP2B1, is
90 responsible for the metabolism of chiral PCBs. These P450 species also metabolize 2,2′,3,6-
91 tetrachlorobiphenyl (CB45), CB91, and CB95 to hydroxylate metabolites enantioselectively.[15]
92 However, structural information of P450 species in predominant formation of metabolites from
93 one atropisomer of chiral PCBs is limited.

94 The objective of this study is to investigate the enantioselective metabolism of CB45 and CB91
95 using human CYP2B6 and rat CYP2B1 with insights from docking models of P450s and each
96 atropisomer. The total production amount of CB45 is approximately 2,000 metric tons that are
97 relatively high among chiral PCBs,[16] and CB91 has been detected in river water.[5] Therefore, the
98 metabolic fate of these PCBs is of great concern. To clarify the mechanisms of enantioselective
99 metabolism, atropisomers isolated from racemic CB45 and CB91 were subjected to metabolism
100 experiments using human CYP2B6 and rat CYP2B1. These approaches easily provide clear

structural insights because docking models of P450s and each atropisomer of chiral PCBs can be constructed. The prediction and identification of the hydroxylation position of CB45 have not yet been reported. Furthermore, the investigated CB congeners were chosen because the difference in one chlorine atom was expected to yield additional information on the effect of structure on the enantioselectivity of CYP-mediated hydroxylation (Figure 1). This provides critical information on the structural relevance of PCB metabolism by P450s.

107

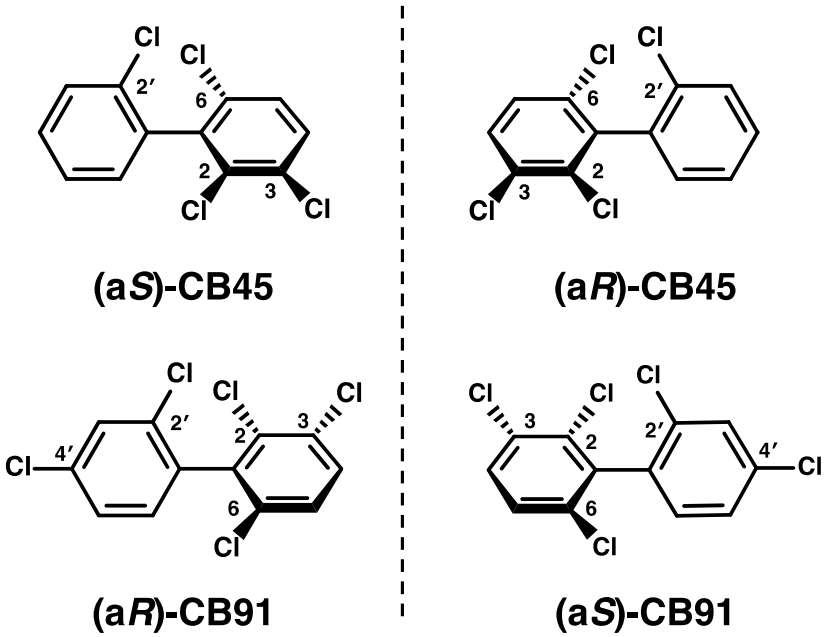

108 **Figure 1** Chemical structures of atropisomers of 2,2′,3,6-tetrachlorobiphenyl (CB45) and
109 2,2′,3,4′,6-pentachlorobiphenyl (CB91).

110

2. MATERIALS AND METHODS

2.1. Chemicals Atropisomers of both CB45 and CB91 were separated from racemic CB45 (≥99% purity) and CB91 (≥99% purity) (AccuStandard, New Haven, CT, USA), respectively, by HPLC on a chiralcel OJ-H column (Daicel Co., Osaka, Japan) under the conditions reported previously (Figure S1).[17] (a*S*)-CB45 and (a*S*)-CB91 were contained in the first elution, and (a*R*)-CB45 and (a*R*)-CB91 were in the second elution (Figure S1A, B).[18] Enantiomeric excess values were determined by the percentage difference of peak areas between atropisomers: (a*S*)-CB45, (a*R*)-CB45, and (a*S*)-CB91 showed 100%, and (a*R*)-CB91 did 98% (Figure S1A, B). Absolute configuration of separated atropisomers of CB45 and CB91 was determined by comparison of experimental and theoretical spectra (Figure S1C, D). Experimental spectrum of the first fraction of CB45 was referred from the result of Guo et al.[18] Experimental spectrum was obtained in hexane (ca. 7.7 μM) for the second fraction of CB91. Theoretical spectra for a*S* and a*R* atropisomers for CB45 and CB91 were calculated at the RI-CC2/aug-def2-TZVPP//B-LYP-D3/def2-TZVP level. The calculated rotational strengths in length gauge were scaled to one-half and were expanded by Gaussian functions and overlapped where the width of the band at 1/e height is fixed at 0.5 eV and the excitation energy was red-shifted by 0.6 eV. The first and second fractions from racemic CB45 and CB91 were determined as (a*S*)-CB45 and (a*S*)-CB91, and (a*R*)-CB45 and (a*R*)-CB91, respectively. Atropisomers of CB45 and CB91 were dissolved in dimethyl sulfoxide (≥99.0% purity, Nacalai Tesque, Inc., Kyoto, Japan) at 3.4 and 3.1 mM, respectively. As an internal standard and a syringe spike, ^{13}C-labeled hydroxylated (OH)-PCBs (MHPCB-MXA: [$^{13}C_{12}$]-4-Hydroxy-3′,4′-dichlorobiphenyl, [$^{13}C_{12}$]-4-hydroxy-2′,4′,5′-trichlorobiphenyl, [$^{13}C_{12}$]-4-hydroxy-2′,3′,4′,5′-tetrachlorobiphenyl, [$^{13}C_{12}$]-4-hydroxy-2′,3,4′,5,5′-pentachlorobiphenyl, [$^{13}C_{12}$]-4-hydroxy-2′,3,3′,4′,5,5′-hexachlorobiphenyl, [$^{13}C_{12}$]-4-hydroxy-2,2′,3,3′,4′,5,5′-heptachlorobiphenyl, and

134 [$^{13}C_{12}$]-4-hydroxy-2,2′,3,4′,5,5′,6-heptachlorobiphenyl), and [$^{13}C_{12}$]-2,3′,4′,5-tetrachlorobiphenyl
135 (CB70) were used (Wellington Laboratories, Guelph, Canada), respectively. The standard 3′-OH-
136 CB51 was kindly provided by Dr. T. Okumura (Environmental Pollution Control Center, Osaka
137 Prefecture, Osaka, Japan). Human CYP2B6 and rat CYP2B1 were used as enzymes heterologously
138 produced in recombinant insect cells, in which microsomes also contain NADPH-cytochrome
139 P450 oxidoreductase and cytochrome b_5 (BD Biosciences, San Jose, CA, USA).

140 **2.2. Monitor of P450-mediated hydroxylation of CB45 and CB91** The reaction solution
141 contained 3.4 μM (a*S*)- or (a*R*)-CB45, or 3.1 μM (a*S*)- or (a*R*)-CB91, P450 enzymes, 3.3 mM
142 $MgCl_2$, 100 mM potassium phosphate buffer (pH 7.4), and NADPH regenerating system (5 mM
143 NADPH, 5 mM glucose-6-phosphate, and 1 unit glucose-6-phosphate dehydrogenase) in a total
144 volume of 0.5 mL. All reagents in the biochemical experiments were purchased from Nacalai
145 Tesque. The reaction was started by adding 80 nM human CYP2B6 or rat CYP2B1, and the
146 mixture was incubated for 120 min at 37°C with continuous shaking. The NADPH-dependent
147 reaction was confirmed using the same reaction mixture without NADPH as a control to show the
148 involvement of P450s to the reactions. The reaction was terminated on ice, and 20 μL of 50 ng/mL
149 ^{13}C-labeled OH-PCB dissolved in acetone (≥99.5% purity, FUJIFILM Wako Pure Chemical Corp.,
150 Osaka, Japan) was added. The hydroxylated metabolites were extracted twice with 2 mL of *n*-
151 hexane (≥96.0% purity, Kanto Chemical Co., Inc., Tokyo, Japan) and derivatized by methylation
152 as described previously.[19] In brief, after dryness of the extracts by nitrogen stream 3 M of
153 KOH/ethanol and dimethyl sulfate were added. The mixture was heated at 70°C for 30 min, and
154 then 10% sodium chloride was added with vigorous mixing. The derivatized metabolites were
155 extracted twice with 2 mL of *n*-hexane. After elimination of water by anhydrous sodium sulfate
156 and addition of *n*-nonane, the volume of the solution was reduced by nitrogen stream. All reagents

in the methylation experiments were purchased from FUJIFILM Wako Pure Chemical. Quantification and identification of the metabolites were performed by gas chromatography and high-resolution mass spectrometry (GC/HRMS) as reported previously (Table S1, S2).[20] In brief, the peak area was measured, and the metabolite amounts were calculated by the calibration curve. However, as there are no commercially available OH-PCB standards, relative amounts of OH-metabolites were calculated from the calibration curve using synthetic standards (Table S3).

2.3. Construction of docking models of human CYP2B6 or rat CYP2B1 and CB45 and CB91 The crystal structure of human CYP2B6 (PDB: 3IBD) was used,[21] and rat CYP2B1 structure was constructed based on the X-ray crystal structure of human CYP2B6 using the "Mutate monomers" tool in SYBYL Biopolymer (Tripos).[22] Docking models of human CYP2B6 and rat CYP2B1 with (a*R*/a*S*)-CB45 and (a*R*/a*S*)-CB91 were constructed using Surflex Dock in SYBYL 8.0 (Tripos, St Louis, MO, USA) as described previously.[23]

2.4. Quality assurance/quality control The biochemical experiments were replicated 4–5 times. Data are presented as mean ± standard deviation for production of metabolites. The recovery rates for hydroxylated metabolites were calculated using an internal standard (^{13}C-labeled OH-PCBs) and a syringe spike ([$^{13}C_{12}$]-CB70) at 55%–157% and 66%–134% for mono-hydroxylated and di-hydroxylated tetrachlorobiphenyls and mono-hydroxylated pentachlorobiphenyls, respectively.

3. RESULTS AND DISSCUSSION

3.1. Detection of CB45 and CB91 metabolites produced using human CYP2B6 and rat CYP2B1 by GC/HRMS For biochemical experiments using recombinant human CYP2B6 and

rat CYP2B1, atropisomers isolated from racemic CB45 and CB91 were used as a substrate. Two different NADPH-dependent mono-OH-tetrachloro metabolites, M1 and M2, were detected from (a*R*)-CB45, and only M1 was detected from (a*S*)-CB45 using microsomes containing human CYP2B6 (Figure 2A). Rat CYP2B1 produced mono-OH-tetrachloro metabolite M1 from both atropisomers (Figure 2B). Three mono-hydroxylated trichloro metabolites, M3–M5, were produced from (a*R*)-CB45 using human CYP2B6 and M5 was produced on using rat CYP2B1 (Figure 2C, D). Two different di-OH-tetrachloro metabolites, M6 and M7, from (a*R*)-CB45 and (a*S*)-CB45, were detected using human CYP2B6 and rat CYP2B1, respectively (Figure 2E, F). From (a*S*)-CB45 and (a*R*)-CB45, no di-OH metabolites were detected using human CYP2B6 and rat CYP2B1, respectively. No obvious peaks representing metabolites were detected when NADPH was not added to the reaction mixture (Figure S2). The recovery rates for hydroxylated metabolites were confirmed using an internal standard and a syringe spike, as describe in the materials and methods.

Three different dechlorinated OH-tetrachloro metabolites, M8, M9, and M10, obtained from CB91 using human CYP2B6 were NADPH-dependent (Figure 3B). From (a*S*)-CB91, M8 and M10 were produced, and M9 and M10 were produced from (a*R*)-CB91. M8 had the same retention time as the standard 3′-MeO-CB51 (Figure 3A, B). In contrast, rat CYP2B1 produced one OH-tetrachloro metabolite, M10, from (a*S*)-CB91 (Figure 3C). Two different OH-pentachloro metabolites, M12 and M13, were detected in a NADPH-dependent manner when human CYP2B6 was used for metabolism of (a*S*)- and (a*R*)-CB91 (Figure 3D). In addition to M12 and M13, M11 was also detected after (a*S*)-CB91 metabolism by rat CYP2B1 (Figure 3E). No metabolite peaks were observed when NADPH was not added (Figure S3).

Retention times and/or retention time indexes were mostly identical among atropisomers metabolized by human CYP2B6 and rat CYP2B1 in each metabolite (Table S3).

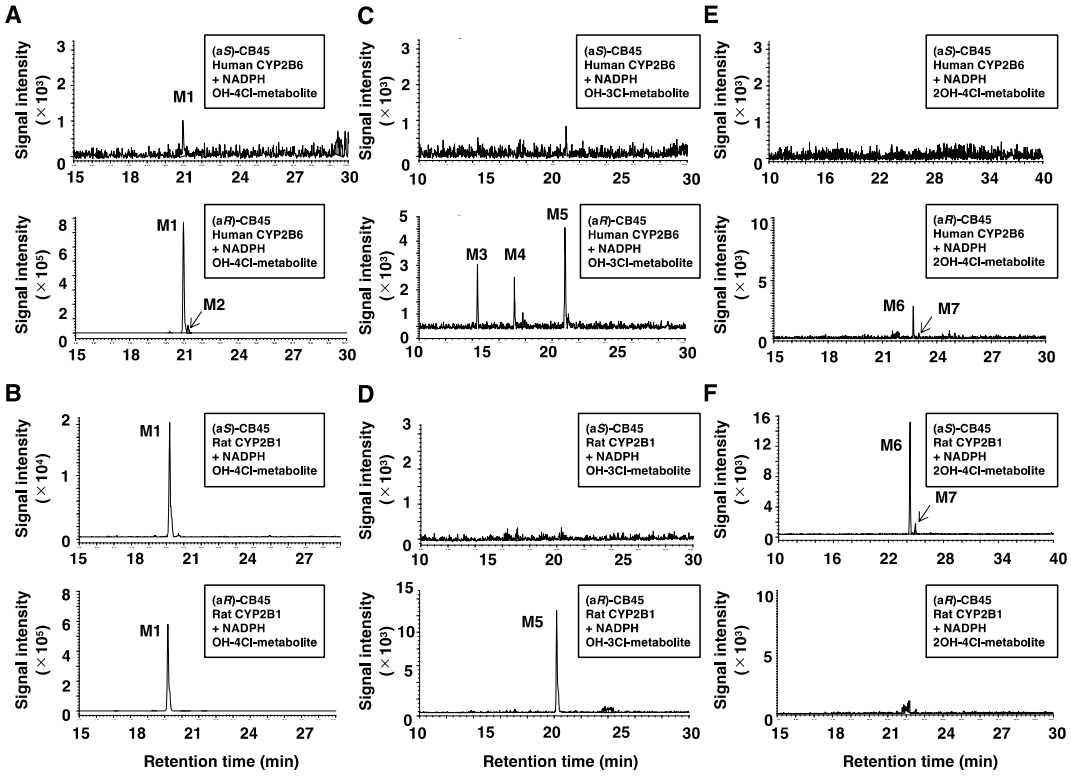

Figure 2 Chromatograms of mono-hydroxylated tetrachloro (A, B), mono-hydroxylated trichloro (C, D), and di-hydroxylated tetrachloro (E, F) metabolites produced from 2,2′,3,6-tetrachlorobiphenyl (CB45) by human CYP2B6 (A, C, E) and rat CYP2B1 (B, D, F), as analyzed by gas chromatography/high-resolution mass spectrometry (GC/HRMS).

The enzymatic reactions with human CYP2B6 and rat CYP2B1 were performed for 120 min at 37°C in the reaction solution contained 3.4 μM (a*S*)- or (a*R*)-CB45, 3.3 mM $MgCl_2$, 100 mM potassium phosphate buffer (pH 7.4), and NADPH regenerating system. The reaction was started by adding 80 nM human CYP2B6 or rat CYP2B1. The hydroxylated metabolites were extracted and derivatized by methylation. Quantification of the metabolites were performed by GC/HRMS. Mono-hydroxylated tetrachloro, mono-hydroxylated trichloro, and di-hydroxylated tetrachloro metabolites are shown as M1 and M2 (A, B), M3–M5 (C, D), and M6 and M7 (E, F), respectively. Upper and lower panels represent the metabolism of (a*S*)-CB45 and (a*R*)-CB45 as substrates, respectively.

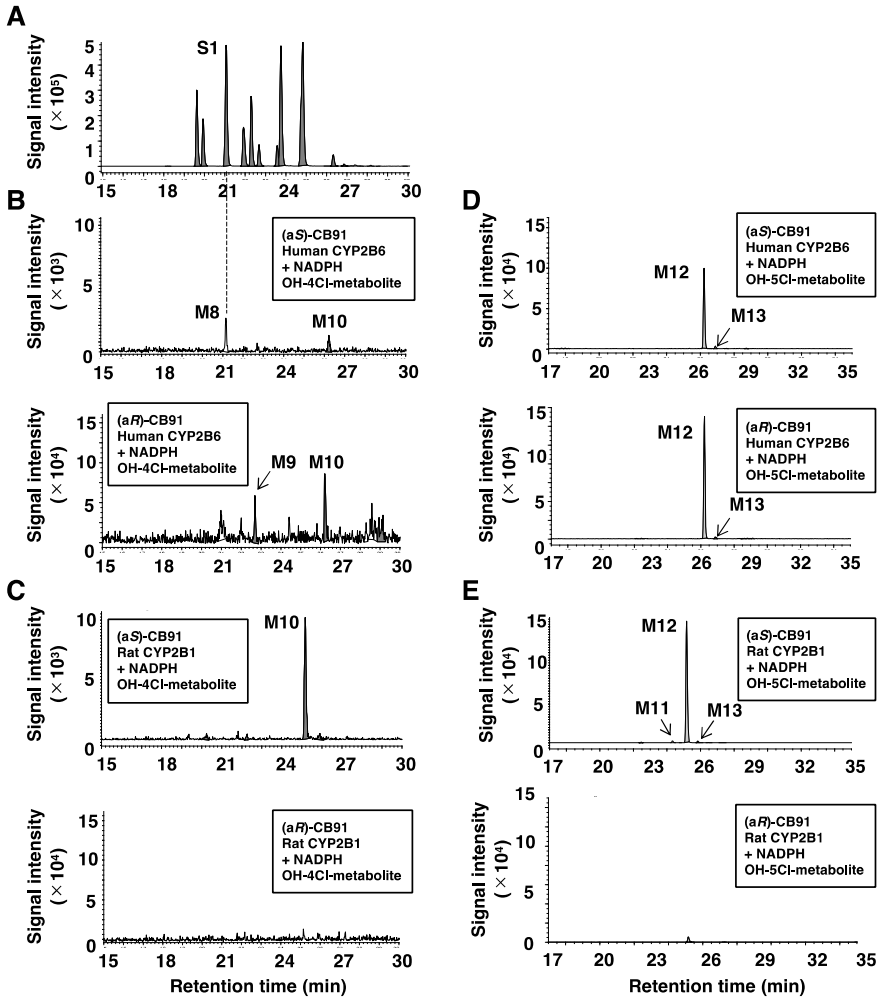

Figure 3 Chromatograms of mono-hydroxylated tetrachloro (B, C) and pentachloro (D, E) metabolites produced from 2,2′,3,4′,6-pentachlorobiphenyl (CB91) by human CYP2B6 (B, D) and rat CYP2B1 (C, E), as analyzed by gas chromatography/high-resolution mass spectrometry (GC/HRMS).

The enzymatic reactions with human CYP2B6 and rat CYP2B1 were performed for 120 min at 37°C in the reaction solution contained 3.1 μM (a*S*)- or (a*R*)-CB91, 3.3 mM $MgCl_2$, 100 mM potassium phosphate buffer (pH 7.4), and NADPH regenerating system. The reaction was started by adding 80 nM human CYP2B6 or rat CYP2B1. The hydroxylated metabolites were extracted and derivatized by methylation. Quantification of the metabolites were performed by GC/HRMS. S1 is the authentic standard, 3′-MeO-2,2′,4,6′-tetrachlorobiphenyl (CB51) (A). Mono-hydroxylated tetrachloro and pentachloro metabolites are shown as M8–10 (B, C) and M11–13 (D,

229 E), respectively. Upper and lower panels represent the metabolism of (a*S*)-CB91 and (a*R*)-CB91
230 as substrates, respectively.

3.2. Prediction and identification of CB45 and CB91 metabolites Isotope ratios of methylated CB45 metabolites were shown in Figure S4 and summarized in Table S4. Actual ratios of the standards were almost identical to the theoretical ratios. The metabolites M1, M2, and M5–M7 showed similar isotope ratios to actual and theoretical ratios. In contrast, isotope ratios of M3 and M4 showed difference to actual and theoretical ratios, indicating that these two metabolites are not OH-metabolites. The patterns of monitored fragment ions of CB45 metabolites showed that M1 and M2 had higher peaks in $[M+2\text{-}COCH_3]^+$ than those in $[M\text{-}ClCH_3]^+$ (Figure S6A–D). When the peak of $[M+2\text{-}COCH_3]^+$ was high, the substituted hydroxyl group existed at the *meta*- or *para*-position.[24] The peak of M5 in $[M\text{-}ClCH_3]^+$ was higher than that in $[M+2\text{-}COCH_3]^+$ (Figure S6E, F). These results indicate that M1 and M2, and M5 have an OH-group at the *meta*- or *para*-, and *ortho*-position, respectively.

Isotope ratios of methylated CB91 metabolites were described in Figure S5 and summarized in Table S4. Similar isotope ratios of the metabolites M8–M13 were observed to theoretical and actual ratios, indicating that these are OH-metabolites. Among OH-tetrachloro metabolites from CB91, M8 and M9 showed higher peaks in $[M+2\text{-}COCH_3]^+$ compared to those in $[M\text{-}ClCH_3]^+$, indicating that these have an OH group at the *meta*- or *para*-position of the biphenyl ring (Figure S7A, B). M8 was identified as 3′-OH-CB51 based on the retention time (Figure 3A, B). Furthermore, M10 showed a reverse pattern as M8 and M9, and M10 had an OH-group at the *ortho*-position (Figure S7A–C). All OH-pentachloro metabolites showed higher peaks in $[M+2\text{-}COCH_3]^+$ than those in $[M\text{-}ClCH_3]^+$, indicating hydroxylation at the *meta*- or *para*-position (Figure S7D, E, F). These results support the structural prediction of M11–M13 from the results of relative amounts of CB91 metabolites in the previous reports.[14]

253 **3.3. Activities on production of CB45 and CB91 metabolites using human CYP2B6 and**
254 **rat CYP2B1** The activity on the production of M1 from (a*R*)-CB45 by human CYP2B6 tended to
255 be much higher than that of other CB45 metabolites (Figure 4A). The major metabolite produced
256 by rat CYP2B1 was also M1 (Figure 4B). However, M2 was not detected in the present study.
257 Mono-OH-trichloro metabolite M5 and di-OH-tetrachloro metabolites M6 and M7 tended to be
258 produced in much less quantities than the mono-OH-tetrachloro metabolites M1 and M2 by human
259 CYP2B6 (Figure 4A, C, E). M2, and M5–M7 were enantioselectively produced from (a*R*)-CB45
260 by human CYP2B6. Mono-OH-trichloro metabolite, M5, was produced from (a*R*)-CB45 with rat
261 CYP2B1 (Figure 4D). Interestingly, M6 and M7 were produced from (a*S*)-CB45 by rat CYP2B1,
262 wherein M6 production tended to be higher than that of M7 (Figure 4F). Di-OH-metabolites were
263 also detected as metabolites of other chiral PCBs, such as CB95, 2,2′,3,3′,4,6′-hexachlorobiphenyl
264 (CB132), CB136, and 2,2′,3,4′,5′,6-hexachlorobiphenyl (CB149).[16] Most CB45 metabolites were
265 produced from (a*R*)-CB45 (Figure 4). Warner et al. reported that CB45 is enantioselectively
266 metabolized by human CYP2B6 and rat CYP2B1, resulting in changes in EFs.[15] In particular, the
267 amount of one atropisomer of CB45 was rapidly reduced by rat CYP2B1, and a high EF value
268 (0.822) of CB45 was observed. These results support our results that the activity on the production
269 of M1 from (a*R*)-CB45 was much higher than that produced from (a*S*)-CB45. However, the
270 changes in EF values on using human CYP2B6 and rat CYP2B1 were opposite[15]; EF values of
271 racemic CB45 were shifted to 0.822 and 0.437 by the incubation of rat CYP2B1 and human
272 CYP2B6, respectively, indicating that different atropisomers were metabolized by these P450s. It
273 may be caused by the metabolic inhibition due to competition between atropisomers in racemic
274 CB45.[25]

The dechlorinated OH-tetrachloro metabolites M8, M9, and M10 tended to be produced by human CYP2B6 to a similar extent (Figure 5A). However, M8 and M9 were not produced from (a*R*)-CB91 and (a*S*)-CB91, respectively. In previous reports of chiral PCB metabolism by P450 species, no dechlorinated metabolites have been reported yet, although dechlorination of PCBs is observed in case of non-chiral 3,3′,4,4′,5-pentachlorobiphenyl (CB126) metabolism by rat CYP1A1.[26] Dechlorination of PCBs decreases their half-life and bioaccumulation as well as hydrophobicity.[27] Therefore, it is one of the important steps to decrease its toxicity. The generated amount of OH-pentachloro metabolite M13 from (a*S*)-CB91 was greater than that produced from (a*R*)-CB91 by human CYP2B6, and the activity on the production of M13 from (a*R*)-CB91 tended to be similar to that of M8, M9, and M10 (Figure 5A, C). The activity on the production of M12 by human CYP2B6 and rat CYP2B1 tended to be much higher than that of other CB91 metabolites (Figure 5C, D). In contrast, activity on the production of M10 on using rat CYP2B1 was comparable to M10 produced by human CYP2B6 (Figure 5A, B). However, M11–13 were more abundantly produced by rat CYP2B1 than human CYP2B6 (Figure 5C, D). Human liver microsomes catalyze the metabolism of CB91 to 3-OH-CB100 as a major metabolite, 5-OH-CB91, and 4-OH-CB91.[28] In contrast, human CYP2B6 produced much higher amounts of 5-OH-CB91 than 4-OH-CB91 and 3-OH-CB100.[14] These results suggest that human CYP2B6 is primarily responsible for the production of 5-OH-CB91, but other P450 species contained in liver microsomes also contribute to CB91 metabolism. Enantioselective production of 5-OH-CB91 was not clearly observed under metabolism by human CYP2B6.[15] In this study, the activity on the production of M12 by human CYP2B6 tended to be higher than that of M13 from (a*S*)-CB91 and (a*R*)-CB91. From the previous results of formation pattern of hydroxylated metabolites, M12 and M13 have been predicted as 5-OH-CB91 and 4-OH-CB91, respectively.[14] In contrast, rat liver

298 microsomes produce 5-OH-CB91 enantioselectively.[29] Furthermore, 5-OH-CB91 is more
299 abundantly produced by rat CYP2B1 compared to other metabolites.[30] These results also support
300 that M12 and M13 are 5-OH-CB91 and 4-OH-CB91, respectively. In addition, M11 was predicted
301 to be 3-OH-CB100 from the relative amount of 3-OH-CB100 to 5-OH-CB91 and 4-OH-CB91.[14]

302

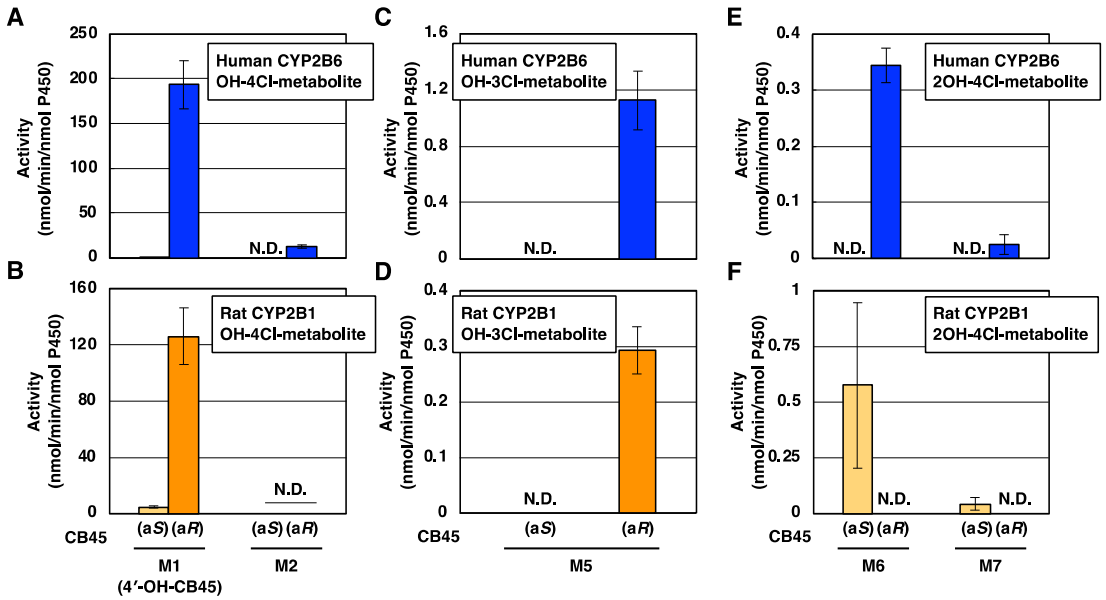

303 **Figure 4** Activity on the production of 2,2′,3,6-tetrachlorobiphenyl (CB45) metabolites using
304 human CYP2B6 (A, C, E) and rat CYP2B1 (B, D, F).
305 The enzymatic reactions with human CYP2B6 and rat CYP2B1 were performed for 120 min at
306 37°C in the reaction solution contained 3.4 μM (a*S*)- or (a*R*)-CB45, 3.3 mM $MgCl_2$, 100 mM
307 potassium phosphate buffer (pH 7.4), and NADPH regenerating system. The reaction was started
308 by adding 80 nM human CYP2B6 or rat CYP2B1. The hydroxylated metabolites were extracted
309 and derivatized by methylation. Quantification of the metabolites were performed by gas
310 chromatography/high-resolution mass spectrometry. Mono-hydroxylated tetrachloro (A, B),
311 mono-hydroxylated trichloro (C, D), and di-hydroxylated tetrachloro (E, F) metabolites were
312 analyzed. Data are presented as mean ± standard deviation (n = 4–5). N.D., not detected. M1 was
313 predicted to be 4′-OH-CB45. As M3 and M4 detected in Figure 2C were not OH-metabolites,
314 activities were not shown in the graph.
315

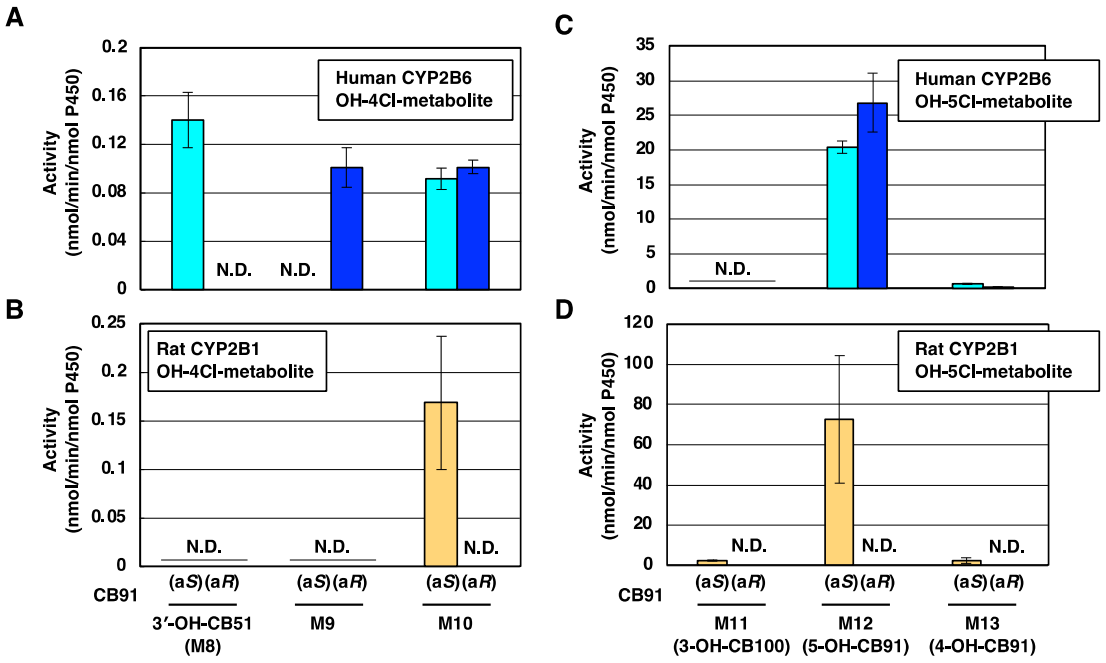

316

317 **Figure 5** Activity on the production of 2,2′,3,4′,6-pentachlorobiphenyl (CB91) metabolites using
318 human CYP2B6 (A, C) and rat CYP2B1 (B, D).
319 The enzymatic reactions with human CYP2B6 and rat CYP2B1 were performed for 120 min at
320 37°C in the reaction solution contained 3.1 μM (a*S*)- or (a*R*)-CB91, 3.3 mM $MgCl_2$, 100 mM
321 potassium phosphate buffer (pH 7.4), and NADPH regenerating system. The reaction was started
322 by adding 80 nM human CYP2B6 or rat CYP2B1. The hydroxylated metabolites were extracted
323 and derivatized by methylation. Quantification of the metabolites were performed by gas
324 chromatography/high-resolution mass spectrometry. Mono-hydroxylated tetrachloro (A, B) and
325 pentachloro (C, D) metabolites were analyzed. Data are presented as mean ± standard deviation (*n*
326 = 5). N.D., not detected. M8 was identified as 3′-OH-2,2′,4,6′-tetrachlorobiphenyl (3′-OH-CB51).
327 M11–13 were predicted as 3-OH-2,2′,4,4′,6-pentachlorobiphenyl (3-OH-CB100), 5-OH-CB91,
328 and 4-OH-CB91, respectively.
329

330

3.4. Docking models of CYP2B subfamilies with CB45 and CB91 In the docking studies of human CYP2B6, two amino acids, F206 and L363, were found to play crucial roles in CB45 conformation in the substrate-binding cavity. Although the 2′-position of (a*S*)-CB45 crashed with L363 in human CYP2B6, the 6′-position of (a*R*)-CB45 did not show any crash (Figure 6A, B). These findings indicate that (a*R*)-CB45 accommodates more stably in the cavity than (a*S*)-CB45, leading to high hydroxylation activity. These results support that the major metabolites are from (a*R*)-CB45 (Figure 4A, C, E). The hydroxylation position of (a*R*)-CB45 was predicted using the docking model of human CYP2B6 (Figure 6C). The stable accommodation of (a*R*)-CB45 in the cavity brings the 4′-position of (a*R*)-CB45 close to heme at 3.1 Å. As a result, it is likely that 4′-OH-CB45, designated as M1, was produced (Figure 6D). This is supported by the results that M1 has an OH-group at the *meta*- or *para*-position (Figure S6). The docking models of rat CYP2B1 toward (a*S*)-CB45 and (a*R*)-CB45 also supported the same results for enantioselective metabolism and the hydroxylation site (Figure S8 and Figure 6C). It is also possible that the 5′ or 3′-position of CB45 preferentially reacts with the resonance effect of the chlorine atom at the 2′-position.

Docking models of human CYP2B6 with (a*S*)-CB91 and (a*R*)-CB91 did not show any structural conflicts in the substrate-binding cavity of human CYP2B6 (Figure 7A). Therefore, there may not be much difference between M12 produced from (a*S*)-CB91 and (a*R*)-CB91 with the help of human CYP2B6 (Figure 5C). M12 and M13 were predicted as 5-OH-CB91 and 4-OH-CB91 by comparing the patterns of the activity with that of the previous reports (Figure 5C and Figure 7B).[14] Docking models showed that the 5-position of CB91 was at a closer distance from heme (6.0 Å) than the 4-position (6.4 Å) (Figure 7A). Because the nearest position to heme can be reacted preferentially, 5-OH-CB91 will be produced more than 4-OH-CB91. The Cl group at the 2′-position of (a*S*)-CB91 was more relaxed in the cavity of rat CYP2B1 than that of (a*R*)-CB91

354 (Figure 7C). It seems that M12 was produced from (a*S*)-CB91 (Figure 5D). Lu et al. reported that
355 the EF value of 5-OH-CB91 is quite low, indicating that one atropisomer of CB91 is primarily
356 metabolized by rat CYP2B1.[30] These results are consistent with our results that (a*S*)-CB91 is
357 enantioselectively metabolized by rat CYP2B1 (Figure 5B, D). Interestingly, the docking model
358 of human CYP2B6 with (a*S*)-CB91 with another conformation revealed that the 3-position of
359 CB91 is close to heme (Figure 7D). This conformation produces two metabolites, 3′-OH-CB51
360 and 3-OH-CB100, designated as M8 and M11, respectively (Figure 7E). This is consistent with
361 the results displayed in Figure S7 and reveal the positions of hydroxylation, indicating that M11
362 has an OH-group at the *meta*- or *para*-position of CB91.

363 CB45 metabolites were highly produced when using human CYP2B6 compared to CB91
364 metabolites (Figure 4A and Figure 5C). One possible explanation is that the distance between
365 CB45 and the heme iron of P450s is much closer than the distance between heme iron and CB91,
366 and CB45 and CB91 are at 3.1 Å and 6.0 Å in the substrate-binding cavity of human CYP2B6,
367 respectively. (Figure 6C and 7A). Close distance creates more opportunities to react, resulting in
368 high amounts of the metabolites.[26] Difference in the distance is due to the different conformations
369 of CB45 and CB91. CB45 is vertically accommodated in the cavity because there is no Cl group
370 at the 4′-position of CB45 compared to CB91, resulting in close distance between it and the heme
371 iron (Figure 6C, Figure 7A).

372 Another important factor related to the activity as well as the distance of PCBs to the heme iron
373 and shape of the substrate-binding cavity configurated by amino acids is a volume of the cavity.
374 Volume can determine the basic size of compounds that can be accommodated. It is reported that
375 human CYP2B6 has a larger volume (559 $Å^3$) than rat CYP2B1 do (472 $Å^3$).[22] The cavity volumes

376 of these P450s are enough large to accommodate CB45 and CB91. The cavity volume and shape
377 are responsible for binding energy of PCBs in the cavity.

378

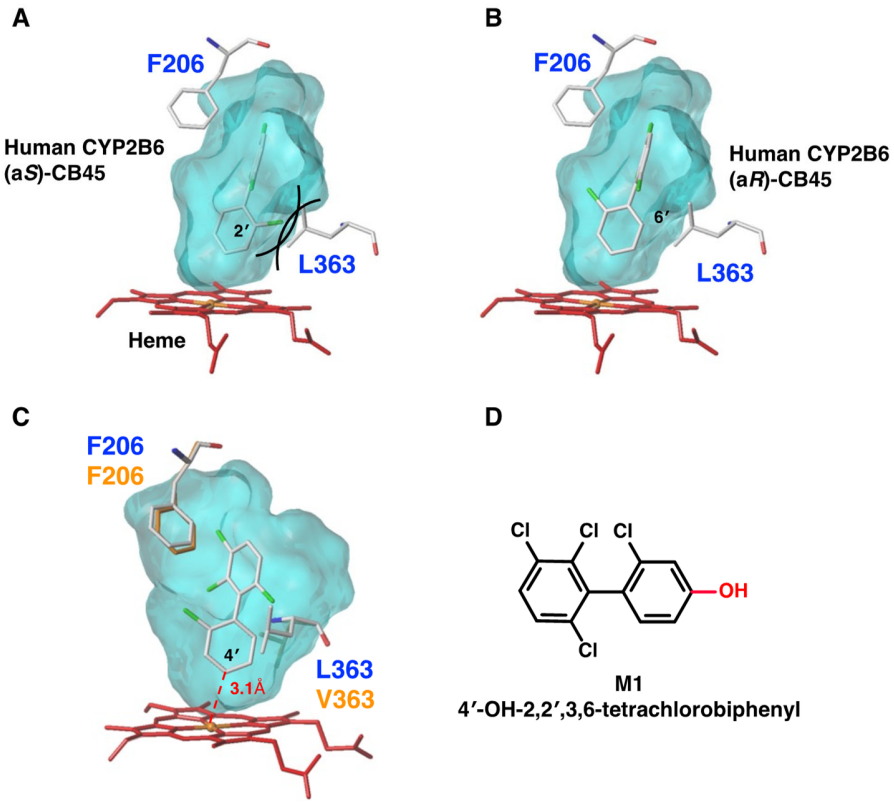

379 **Figure 6** Preference of (a*R*)-2,2′,3,6-tetrachlorobiphenyl (CB45) metabolism and a predicted
380 hydroxylated metabolite produced by human CYP2B6.
381 Docking models of human CYP2B6 toward (a*S*)-CB45 (A) and (a*R*)-CB45 (B) are described. The
382 green stick in CB45 indicates a chlorine atom. Amino acids described in blue and orange constitute
383 the human and rat substrate-binding cavities, respectively. Steric hindrance between chlorine at
384 the 2′-position of (a*S*)-CB45 and a side chain of amino acids, such as L363, constituting the human
385 CYP2B6 cavity, is observed. Human and rat substrate-binding cavities are superimposed, and the
386 distance between the 4′-position of the main conformation of (a*R*)-CB45 and heme iron is specified
387 (C). M1 was predicted to be 4′-OH-CB45 (D).
388

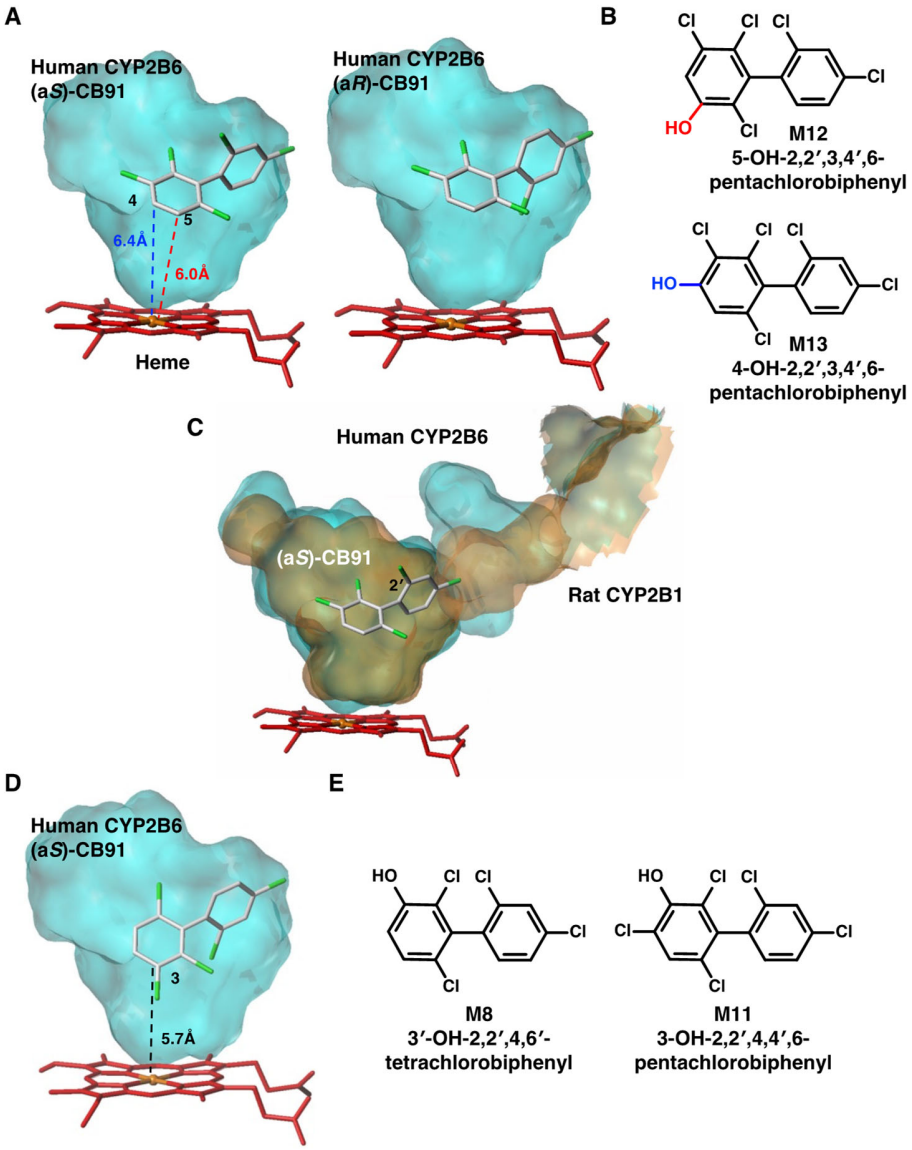

389 **Figure 7** Structural basis of 2,2′,3,4′,6-pentachlorobiphenyl (CB91) metabolism and predicted
390 hydroxylated metabolites on using human CYP2B6.
391 The docking models of (a*S*)-CB91 and (a*R*)-CB91 with human CYP2B6 to predict M12 and M13
392 are described (A, B). The substrate-binding cavities of human CYP2B6 (light blue) and rat
393 CYP2B1 (orange) docked with (a*S*)-CB91 are superimposed (C). The docking model of human
394 CYP2B6 with (a*S*)-CB91 to show M8 and M11 is described (D, E). Green bars in CB91 indicate
395 chlorine atoms. M8 was identified as 3′-OH-2,2′,4,6′-tetrachlorobiphenyl (3′-OH-CB51). M11–13
396 were predicted to be 3-OH-2,2′,4,4′,6-pentachlorobiphenyl (3-OH-CB100), 5-OH-CB91, and 4-
397 OH-CB91, respectively.

3.5. Proposed pathways of metabolism of CB45 and CB91 by human CYP2B6 and rat CYP2B1 The major mono-OH-tetrachloro metabolite of CB45 produced by human CYP2B6 is M1, which is predicted to be 4′-OH-CB45 (Figure 8). This metabolite was enantioselectively produced from (a*R*)-CB45. It is presumed that M2 undergoes *meta*-hydroxylation of the monochlorophenyl ring or *meta*- or *para*-hydroxylation of the trichlorophenyl ring. Furthermore, it is presumed that some of the mono-OH-metabolites are intermediates of di-OH-metabolites M6 and M7. Dechlorination with hydroxylation is another pathway to produce M5, albeit minor. Most CB45 metabolites are produced from (a*R*)-CB45.

CB91 is primarily metabolized to M12, predicted as 5-OH-CB91, and was enantioselective metabolized by rat CYP2B1 but not by human CYP2B6 (Figure 9). It has also been observed *in vivo* that CB91 detected in breast milk showed nearly racemic composition in all samples.[31] 3′-OH-CB51 designated as M8 was the sole identified metabolite of CB91. Some metabolites, such as M10 and M12, produced by human CYP2B6 did not exhibit enantioselectivity. Moreover, it has been reported that the substrate-binding cavity of human CYP2B6 is larger than that of rat CYP2B1.[22] Large cavity may accommodate both atropisomers without any atropisomer-specific steric hindrance. The structures of the metabolites M11–M13 were predicted by our results and previous results.[14,15,30]

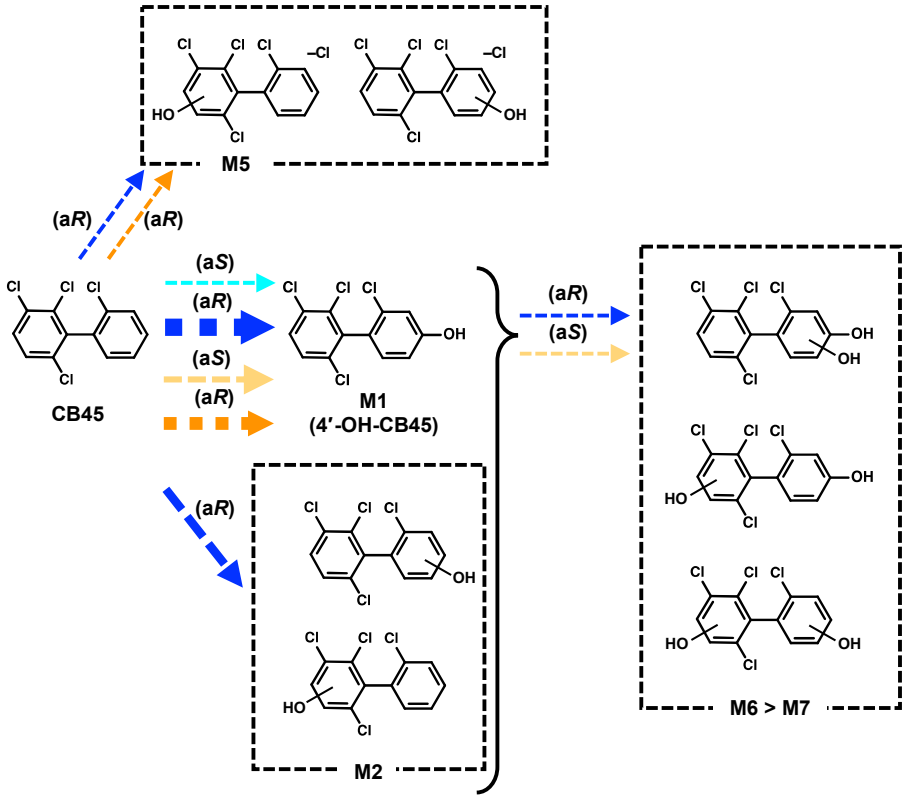

Figure 8 Proposed metabolic pathways for metabolism of 2,2′,3,6-tetrachlorobiphenyl (CB45) by human CYP2B6 and rat CYP2B1.

Enantioselective metabolism is shown as arrow thickness, which indicates the approximate level of hydroxylation activity. Blue/light blue and orange/light orange dotted arrows indicate the predicted metabolic pathways by human CYP2B6 and rat CYP2B1, respectively. Light blue and light orange, and blue and orange arrows indicate the pathways for (a*S*)-CB45 and (a*R*)-CB45, respectively. Red points on the biphenyl ring indicate possible hydroxylation sites. The amount of M6 was higher than that of M7. M1 was predicted to be 4′-OH-CB45 from the docking model of human CYP2B6 with CB45.

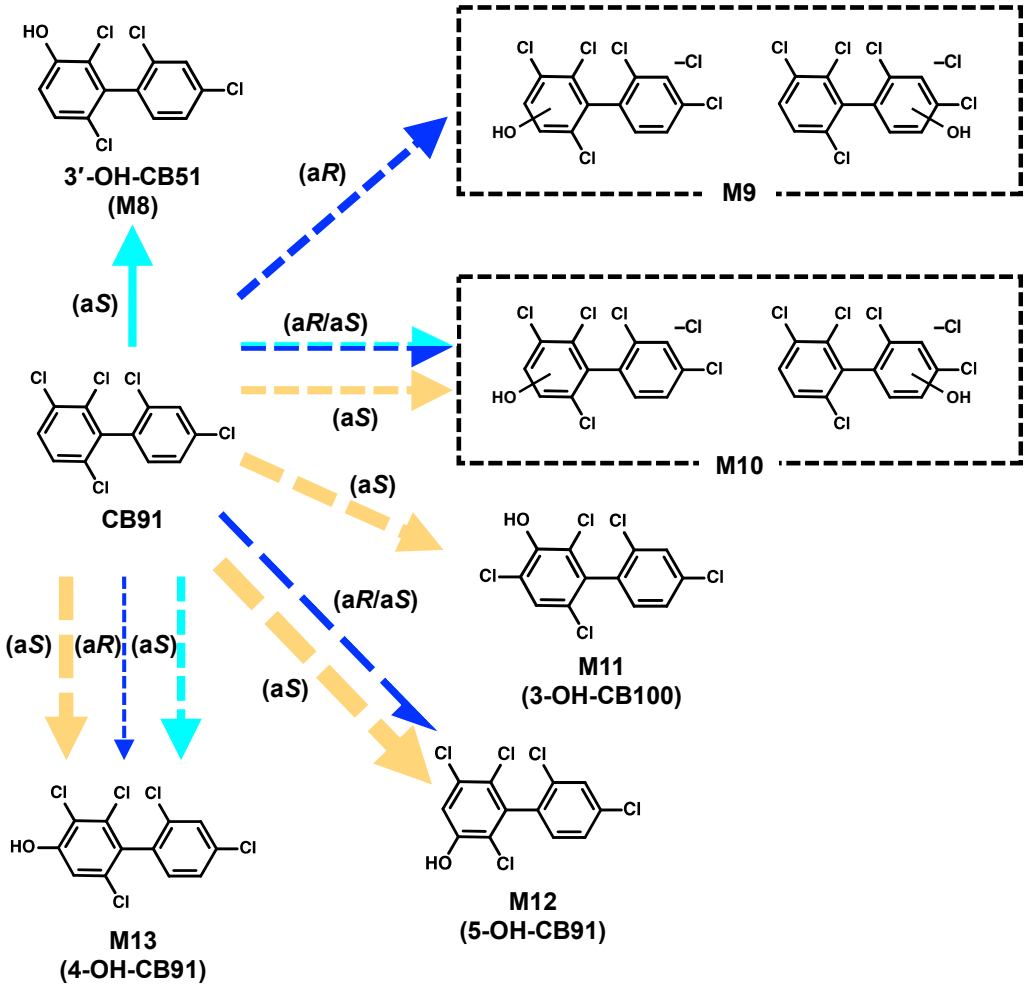

425 **Figure 9** Proposed metabolic pathways for metabolism of 2,2′,3,4′,6-pentachlorobiphenyl (CB91)
426 by human CYP2B6 and rat CYP2B1.
427 Arrow thickness shows enantioselective metabolism, indicating the approximate level of
428 hydroxylation activity. Blue and light blue, and light orange dotted arrows indicate the predicted
429 metabolic pathways by human CYP2B6 and rat CYP2B1, respectively. Light blue and light orange,
430 and blue arrows indicate the pathways for (a*S*)-CB91 and (a*R*)-CB91, respectively. Red points on
431 the biphenyl ring indicate possible hydroxylation sites. M8 was identified as 3′-OH-2,2′,4,6′-
432 tetrachlorobiphenyl (3′-OH-CB51), as indicated by the solid light blue arrow. M11–13 were
433 predicted to be 3-OH-2,2′,4,4′,6-pentachlorobiphenyl (3-OH-CB100), 5-OH-CB91, and 4-OH-
434 CB91, respectively.

3.6. Implications from structural basis of atropisomer-specific metabolism of chiral PCBs

Either of the atropisomers often have stronger toxicity than the other one and can suppress the toxicity derived from another one, leading to racemic chiral PCBs and their atropisomers showing different toxicities.[32] Chiral environments lead to enantioselective metabolism. Therefore, it is important to reveal the metabolic fate of each atropisomer in chiral PCBs. Furthermore, since differences in metabolic fates between human and experimental animals influence the extrapolation of the health risk of chiral PCBs, the mechanisms underlying species differences should be clarified.

In this study, using human CYP2B6 and rat CYP2B1, it was revealed that each atropisomer of CB45 and CB91 enters different metabolic pathways. Although there are several reports on CB45 and CB91 metabolism *in vitro*, to the best of our knowledge, this is the first report on the use of isolated atropisomers of CB45 and CB91 as substrates for metabolism experiments. This approach contributes to the understanding of the detailed metabolic mechanisms. In addition, it provides a clear explanation for the structural basis of enantioselective metabolism by P450 species. Thus, this study makes it possible to predict the metabolic fate of other structurally related chiral PCBs. It is thought that dechlorinated and hydroxylated PCBs usually exhibit decreased toxicity due to their increased sensitivity to further metabolic systems, such as conjugation. However, some hydroxylated metabolites of chiral PCBs have high binding affinity to RyR, resulting in increased toxicity.[4] In contrast, di-OH-metabolites showed less binding affinity. As di-OH-metabolites were detected on CB45 metabolism in this study, further hydroxylation of mono-OH-metabolites, eventually leading to a decrease in toxicity, should be evaluated in future docking studies of mono-OH-metabolites to P450s. While the docking models presented herein based on the reported crystal structures require additional experimental validation, such as co-crystallized structural elucidation,

458 this study provides significant insights on the enantioselective metabolism of chiral CBs with the
459 human and rat CYPs.

460

461

462 **Supporting Information**

463 Isolation of atropisomers from racemic CB45 and CB91 and their CD spectra; chromatograms of
464 mono-hydroxylated tetrachloro, mono-hydroxylated trichloro, and di-hydroxylated tetrachloro
465 metabolites produced from CB45 by human CYP2B6 and rat CYP2B1; chromatograms of mono-
466 hydroxylated tetrachloro and pentachloro metabolites produced from CB91 by human CYP2B6
467 and rat CYP2B1; isotope ratios of methylated CB45 metabolites produced by human CYP2B6 and
468 rat CYP2B1; isotope ratios of methylated CB91 metabolites produced by human CYP2B6 and rat
469 CYP2B1; patterns of fragment ions of mono-hydroxylated tetrachloro metabolites of (a*S*)-CB45
470 and (a*R*)-CB45 and mono-hydroxylated trichloro metabolites of (a*R*)-CB45 produced on using
471 human CYP2B6 and rat CYP2B1; patterns of fragment ions of mono-hydroxylated tetrachloro and
472 pentachloro metabolites of (a*S*)-CB91 and (a*R*)-CB91 produced on using human CYP2B6 and rat
473 CYP2B1; preferential metabolism of (a*R*)-CB45 by rat CYP2B1; analysis conditions for
474 derivatized hydroxylated PCBs by gas chromatography/high-resolution mass spectrometry;
475 monitored ions of derivatized hydroxylated PCBs by gas chromatography/high-resolution mass
476 spectrometry; retention times and retention time indexes for hydroxylated metabolites of CB45
477 and CB91; and isotope ratios of hydroxylated metabolites of CB45 and CB91.

478

479 ***Corresponding Author**

Hideyuki Inui, Biosignal Research Center, Kobe University, 1-1 Rokkodaicho, Nada-ku, Kobe, Hyogo, 657-8501, Japan

E-mail: hinui@kobe-u.ac.jp, Telephone number: +81-78-803-5863

Author Contributions

TI, CM, SM, EG, and HT performed metabolism experiments and collected data. YH, CM, and TN performed the experiments and collected data. MK, TI, and KY constructed docking models. MM and TM measured spectra and analyzed. TI, HT, and HI drafted the manuscript. HI designed the study.

Funding Sources

This work was supported by a Grant-in-Aid for Challenging Exploratory Research (grant number 25550064) from the Japan Society for the Promotion of Science to HI and by a CREST (grant number JPMJCR2001) from Japan Science and Technology Agency to TM.

Notes

The authors declare no competing financial interest.

Acknowledgment

We thank Dr. Tameo Okumura of the Environmental Pollution Control Center (Osaka Prefecture, Osaka, Japan) for kindly providing us with the standard 3′-OH-CB51.

REFERENCES

(1) Anzenbacher, P.; Anzenbacherová, E. Cellular and Molecular Life Sciences Cytochromes P450 and Metabolism of Xenobiotics. *Cell. Mol. Life Sci.* **2001**, *58* (5–6), 737–747. https://doi.org/10.1007/PL00000897

(2) Hens, B.; Hens, L. Persistent Threats by Persistent Pollutants: Chemical Nature, Concerns and Future Policy Regarding PCBs—What Are We Heading For? *Toxics* **2018**, *6* (1), 1–21. https://doi.org/10.3390/toxics6010001.

(3) Van den Berg, M.; Birnbaum, L. S.; Denison, M.; De Vito, M.; Farland, W.; Feeley, M.; Fiedler, H.; Hakansson, H.; Hanberg, A.; Haws, L.; Rose, M.; Safe, S.; Schrenk, D.; Tohyama, C.; Tritscher, A.; Tuomisto, J.; Tysklind, M.; Walker, N.; Peterson, R. E. The 2005 World Health Organization Reevaluation of Human and Mammalian Toxic Equivalency Factors for Dioxins and Dioxin-like Compounds. *Toxicol. Sci.* **2006**, *93* (2), 223–241. https://doi.org/10.1093/toxsci/kfl055.

(4) Pessah, I. N.; Hansen, L. G.; Albertson, T. E.; Garner, C. E.; Ta, T. A.; Do, Z.; Kim, K. H.; Wong, P. W. Structure-Activity Relationship for Noncoplanar Polychlorinated Biphenyl Congeners toward the Ryanodine Receptor-Ca^{2+} Channel Complex Type 1 (RyR1). *Chem. Res. Toxicol.* **2006**, *19* (1), 92–101. https://doi.org/10.1021/tx050196m.

(5) Dang, V. D.; Walters, D. M.; Lee, C. M. Assessing Ongoing Sources of Dissolved-Phase Polychlorinated Biphenyls in a Contaminated Stream. *Environ. Toxicol. Chem.* **2013**, *32* (3), 535–540. https://doi.org/10.1002/etc.2106.

(6) He, Z.; Wang, Y.; Zhang, Y.; Cheng, H.; Liu, X. Stereoselective Bioaccumulation of Chiral PCB 91 in Earthworm and Its Metabolomic and Lipidomic Responses. *Environ. Pollut.* **2018**, *238*, 421–430. https://doi.org/10.1016/j.envpol.2018.03.060.

(7) Chai, T.; Cui, F.; Mu, X.; Yang, Y.; Qi, S.; Zhu, L.; Wang, C.; Qiu, J. Stereoselective Induction by 2,2,3,4,6-Pentachlorobiphenyl in Adult Zebrafish (*Danio rerio*): Implication of Chirality in Oxidative Stress and Bioaccumulation. *Environ. Pollut.* **2016**, *215*, 66–76. https://doi.org/10.1016/j.envpol.2016.04.075.

(8) Hoekstra, P. F.; Wong, C. S.; O'Hara, T. M.; Solomon, K. R.; Mabury, S. A.; Muir, D. C. G. Enantiomer-Specific Accumulation of PCB Atropisomers in the Bowhead Whale (*Balaena mysticetus*). *Environ. Sci. Technol.* **2002**, *36* (7), 1419–1425. https://doi.org/10.1021/es015763g.

(9) Konishi, Y.; Kakimoto, K.; Nagayoshi, H.; Nakano, T. Trends in the Enantiomeric Composition of Polychlorinated Biphenyl Atropisomers in Human Breast Milk. *Environ. Sci. Pollut. Res.* **2016**, *23* (3), 2027–2032. https://doi.org/10.1007/s11356-015-4620-6.

(10) Chai, T.; Cui, F.; Song, Y.; Ye, L.; Li, T.; Qiu, J.; Liu, X. Enantioselective Toxicity in Adult Zebrafish (*Danio rerio*) Induced by Chiral PCB91 through Multiple Pathways. *Environ. Sci. Technol.* **2018**, *52* (9), 5448–5458. https://doi.org/10.1021/acs.est.8b00023.

(11) Yang, D.; Kania-Korwel, I.; Ghogha, A.; Chen, H.; Stamou, M.; Bose, D. D.; Pessah, I. N.; Lehmler, H. J.; Lein, P. J. PCB 136 Atropselectively Alters Morphometric and Functional Parameters of Neuronal Connectivity in Cultured Rat Hippocampal Neurons via Ryanodine Receptor-Dependent Mechanisms. *Toxicol. Sci.* **2014**, *138* (2), 379–392. https://doi.org/10.1093/toxsci/kft334.

(12) Uwimana, E.; Maiers, A.; Li, X.; Lehmler, H. J. Microsomal Metabolism of Prochiral Polychlorinated Biphenyls Results in the Enantioselective Formation of Chiral Metabolites. *Environ. Sci. Technol.* **2017**, *51* (3), 1820–1829. https://doi.org/10.1021/acs.est.6b05387.

(13) Wu, X.; Duffel, M.; Lehmler, H. J. Oxidation of Polychlorinated Biphenyls by Liver Tissue Slices from Phenobarbital-Pretreated Mice Is Congener-Specific and Atropselective. *Chem. Res. Toxicol.* **2013**, *26* (11), 1642–1651. https://doi.org/10.1021/tx400229e.

(14) Uwimana, E.; Ruiz, P.; Li, X.; Lehmler, H. J. Human CYP2A6, CYP2B6, and CYP2E1 Atropselectively Metabolize Polychlorinated Biphenyls to Hydroxylated Metabolites. *Environ. Sci. Technol.* **2019**, *53*, 2114–2123. https://doi.org/10.1021/acs.est.8b05250.

(15) Warner, N. A.; Martin, J. W.; Wong, C. S. Chiral Polychlorinated Biphenyls Are Biotransformed Enantioselectively by Mammalian Cytochrome P-450 Isozymes to Form Hydroxylated Metabolites. *Environ. Sci. Technol.* **2009**, *43* (1), 114–121. https://doi.org/10.1021/es802237u.

(16) Kania-Korwel, I.; Lehmler, H. J. Chiral Polychlorinated Biphenyls: Absorption, Metabolism and Excretion—a Review. *Environ. Sci. Pollut. Res.* **2016**, *23* (3), 2042–2057. https://doi.org/10.1007/s11356-015-4150-2.

(17) Toda, M.; Matsumura, C.; Tsurukawa, M.; Okuno, T.; Nakano, T.; Inoue, Y.; Mori, T. Absolute Configuration of Atropisomeric Polychlorinated Biphenyl 183 Enantiomerically Enriched in Human Samples. *J. Phys. Chem. A* **2012**, *116* (37), 9340–9346. https://doi.org/10.1021/jp306363n.

(18) Guo, F.; Tang, Q.; Xie, J.; Zhao, L.; Liu, K.; Liu, W. Enantioseparation and Identification for the Rationalization of the Environmental Impact of 4 Polychlorinated Biphenyls. *Chirality* **2018**, *30* (4), 475–483. https://doi.org/10.1002/chir.22811.

(19) Sakiyama, T., Yamamoto, A., Kakutani, N., Fukuyama, J., and Okumura, T. Hydroxylated Polychlorinated Biphenyls (OH-PCBs) in the Aquatic Environment: Levels and Congener Profiles in Sediments from Osaka, Japan. *Organohal. Comp.* **2007**, *69* (2007), 1380–1383.

(20) Goto, E.; Haga, Y.; Kubo, M.; Itoh, T.; Kasai, C.; Shoji, O.; Yamamoto, K.; Matsumura, C.; Nakano, T.; Inui, H. Metabolic Enhancement of 2,3″,4,4″,5-Pentachlorobiphenyl (CB118) Using Cytochrome P450 Monooxygenase Isolated from Soil Bacterium under the Presence of Perfluorocarboxylic Acids (PFCAs) and the Structural Basis of Its Metabolism. *Chemosphere* **2018**, *210*, 376–383. https://doi.org/10.1016/j.chemosphere.2018.07.026.

(21) Gay, S. C.; Shah, M. B.; Talakad, J. C.; Maekawa, K.; Roberts, A. G.; Wilderman, P. R.; Sun, L.; Yang, J. Y.; Huelga, S. C.; Hong, W. X.; Zhang, Q.; Stout, C. D.; Halpert, J. R. Crystal Structure of a Cytochrome P450 2B6 Genetic Variant in Complex with the Inhibitor 4-(4-Chlorophenyl)Imidazole at 2.0-Å Resolution. *Mol. Pharmacol.* **2010**, *77* (4), 529–538. https://doi.org/10.1124/mol.109.062570.

(22) Mise, S.; Haga, Y.; Itoh, T.; Kato, A.; Fukuda, I.; Goto, E.; Yamamoto, K.; Yabu, M.; Matsumura, C.; Nakano, T.; Sakaki, T.; Inui, H. Structural Determinants of the Position of 2,3′,4,4′,5-Pentachlorobiphenyl (CB118) Hydroxylation by Mammalian Cytochrome P450 Monooxygenases. *Toxicol. Sci.* **2016**, *152* (2), 340–348. https://doi.org/10.1093/toxsci/kfw086.

(23) Ruppert, J.; Welch, W.; Jain, A. N. Automatic Identification and Representation of Protein Binding Sites for Molecular Docking. *Protein Sci.* **1997**, *6* (3), 524–533. https://doi.org/10.1002/pro.5560060302.

588 (24) Kunisue, T.; Tanabe, S. Hydroxylated Polychlorinated Biphenyls (OH-PCBs) in the Blood
589 of Mammals and Birds from Japan: Lower Chlorinated OH-PCBs and Profiles.
590 *Chemosphere* **2009**, *74* (7), 950–961. https://doi.org/10.1016/j.chemosphere.2008.10.038.
591 (25) Lu, Z.; Wong, C. S. Factors Affecting Phase I Stereoselective Biotransformation of Chiral
592 Polychlorinated Biphenyls by Rat Cytochrome P-450 2B1 Isozyme. *Environ. Sci. Technol.*
593 **2011**, *45* (19), 8298–8305. https://doi.org/10.1021/es200673q.
594 (26) Yamazaki, K.; Suzuki, M.; Itoh, T.; Yamamoto, K.; Kanemitsu, M.; Matsumura, C.;
595 Nakano, T.; Sakaki, T.; Fukami, Y.; Imaishi, H.; Inui, H. Structural Basis of Species
596 Differences between Human and Experimental Animal CYP1A1s in Metabolism of
597 3,3′,4,4′,5-Pentachlorobiphenyl. *J. Biochem.* **2011**, *149* (4).
598 https://doi.org/10.1093/jb/mvr009.
599 (27) Tang, B.; Luo, X. J.; Zeng, Y. H.; Mai, B. X. Tracing the Biotransformation of PCBs and
600 PBDEs in Common Carp (*Cyprinus carpio*) Using Compound-Specific and Enantiomer-
601 Specific Stable Carbon Isotope Analysis. *Environ. Sci. Technol.* **2017**, *51* (5), 2705–2713.
602 https://doi.org/10.1021/acs.est.6b05130.
603 (28) Uwimana, E.; Li, X.; Lehmler, H. J. Human Liver Microsomes Atropselectively
604 Metabolize 2,2′,3,4′,6-Pentachlorobiphenyl (PCB 91) to a 1,2-Shift Product as the Major
605 Metabolite. *Environ. Sci. Technol.* **2018**, *52* (10), 6000–6008.
606 https://doi.org/10.1021/acs.est.8b00612.
607 (29) Kania-Korwel, I.; Duffel, M. W.; Lehmler, H. J. Gas Chromatographic Analysis with
608 Chiral Cyclodextrin Phases Reveals the Enantioselective Formation of Hydroxylated
609 Polychlorinated Biphenyls by Rat Liver Microsomes. *Environ. Sci. Technol.* **2011**, *45* (22),
610 9590–9596. https://doi.org/10.1021/es2014727.

(30) Lu, Z.; Kania-Korwel, I.; Lehmler, H. J.; Wong, C. S. Stereoselective Formation of Mono- and Dihydroxylated Polychlorinated Biphenyls by Rat Cytochrome P450 2B1. *Environ. Sci. Technol.* **2013**, *47* (21), 12184–12192. https://doi.org/10.1021/es402838f.

(31) Bordajandi, L. R.; Abad, E.; González, M. J. Occurrence of PCBs, PCDD/Fs, PBDEs and DDTs in Spanish Breast Milk: Enantiomeric Fraction of Chiral PCBs. *Chemosphere* **2008**, *70* (4), 567–575. https://doi.org/10.1016/j.chemosphere.2007.07.019.

(32) Feng, W.; Zheng, J.; Robin, G.; Dong, Y.; Ichikawa, M.; Inoue, Y.; Mori, T.; Nakano, T.; Pessah, I. N. Enantioselectivity of 2,2′,3,5′,6-Pentachlorobiphenyl (PCB 95) Atropisomers toward Ryanodine Receptors (RyRs) and Their Influences on Hippocampal Neuronal Networks. *Environ. Sci. Technol.* **2017**, *51* (24), 14406–14416. https://doi.org/10.1021/acs.est.7b04446.

626 **GRAPHIC FOR TABLE OF CONTENTS**

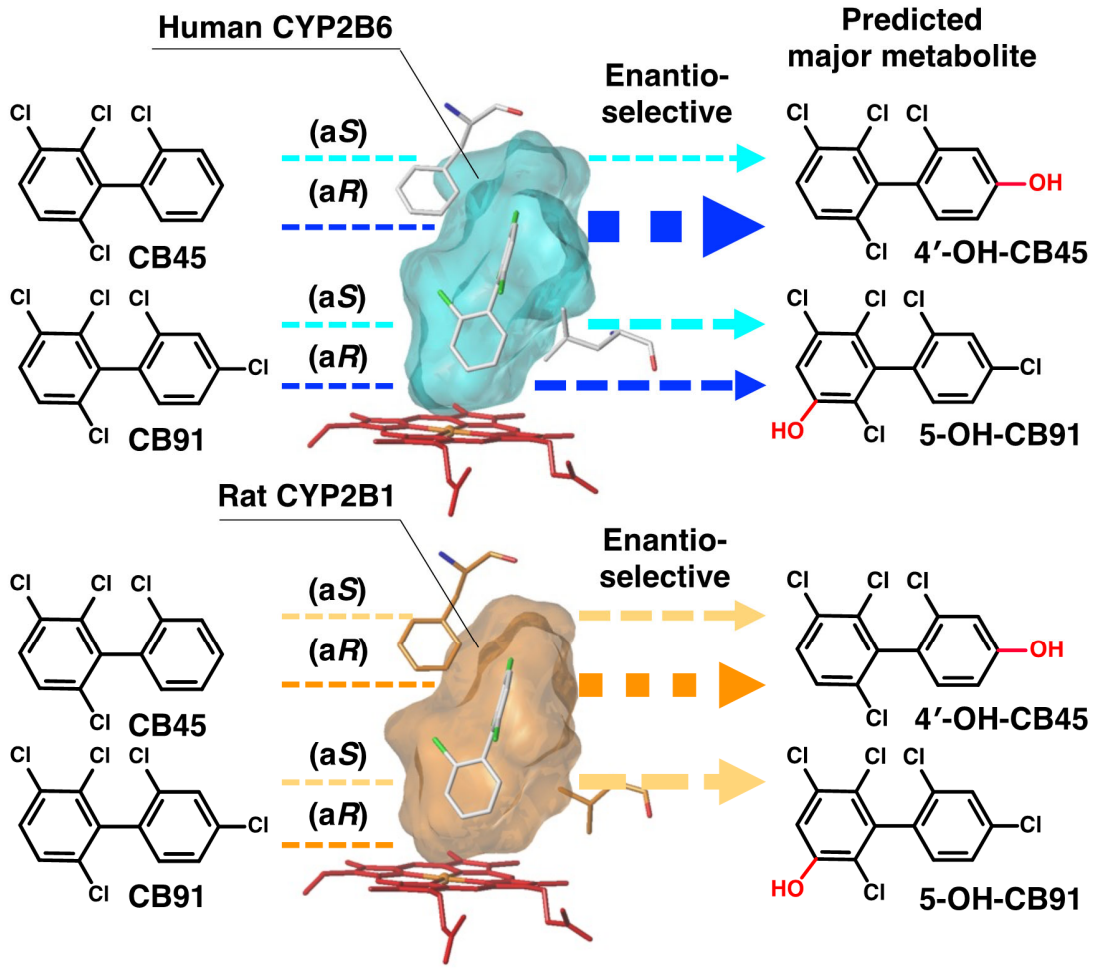

627